Cellulose (2017) 24:5495–5503
DOI 10.1007/s10570-017-1532-2

ORIGINAL PAPER

Thermodynamic effect on interaction between crystalline phases in size-controlled ACC-bacterial nanocellulose and poly(vinyl alcohol)

Gento Ishikawa · Tetsuo Kondo

Received: 18 February 2017 / Accepted: 16 October 2017 / Published online: 27 October 2017

Abstract The aqueous counter collision (ACC) method can provide single bacterial nanocellulose ribbons (ACC-BNC) in a desired width, from a pellicle produced by *Gluconacetobacter xylinus*. Kose et al. (Biomacromolecules, 12:716–720, 2011) reported that the ACC process transformed the major I_α crystalline phase of the native fiber to a stable I_β phase, without decreasing the overall crystallinity. The current study investigated the variation of the crystalline phases of ACC-BNC, upon interaction with poly(vinyl alcohol) (PVA). ACC-BNC of desired width was mixed with PVA, without any chemical reaction occurring. This resulted in a homogeneous suspension. The equilibrium melting point of PVA in cast nanocomposite films was investigated, as a probe for evaluating the crystalline surface properties of the ACC-BNC. A decrease in the equilibrium melting point of PVA would have indicated attractive interactions between the PVA and ACC-BNC. However, the nature of the ACC-BNC surface in the presence of PVA depended on the ACC-BNC width. Thicker ACC-BNC acted as a nucleating agent for PVA. Thinner ACC-BNC acted as a diluent of PVA. This tendency was opposite to the case for I_β-dominant ACC-wood nanocellulose. ACC-BNC acting as a nucleating agent was more efficient than ACC-wood nanocellulose. The results suggested that ACC-BNC surfaces, which probably contained I_α phases, had different characteristics to those of I_β-dominant ACC-wood nanocellulose surfaces.

Keywords Bacterial nanocellulose · Aqueous counter collision · Nano-size effect · Nanocomposite · Crystalline phase

G. Ishikawa · T. Kondo (✉)
Graduate School of Bioresource and Bioenvironmental Sciences, Kyushu University, 6-10-1 Hakozaki, Fukuoka 812-8581, Japan
e-mail: tekondo@agr.kyushu-u.ac.jp

Introduction

Nanocellulose, or cellulose nanofiber, can be produced from various native cellulose sources. The crystalline structures of these sources differ, because of their varying cellulose biosynthesis processes (Moon et al. 2011). In the vascular bundle, the wood cell wall is formed from the cellulose I_β crystalline phase (Wada et al. 1997). The Microorganism *Gluconacetobacter xylinus* produces a composite of cellulose I_α and I_β crystalline phases (Attala and Vanderhart 1984; Yamamoto et al. 1996). Regardless of the specific crystalline structure, the application of nanocellulose has attracted increasing recent attention (Klemm et al. 2011).

Bacterial nanocellulose (BNC) secreted by *G. xylinus* has received much attention because of its useful properties. It exhibits a small coefficient of thermal expansion along its axial direction (0.1 ppm/

K), a high Young's modulus (~ 138 GPa), and a high tensile strength (~ 2 GPa) (Yano et al. 2005; Ifuku et al. 2007). The native three-dimensional (3D)-network structure of BNC, known as pellicle, possesses a high surface area (Vitta and Thiruvengadam 2012), high water absorption capacity (Yamanaka et al. 1989), biodegradability and biocompatibility (Helenius et al. 2006). To exploit these properties, BNC has been extensively studied in applications including tissue engineering, wound dressing, drug delivery, filtration, electronic devices, and polymer nanocomposites (Shah et al. 2013; Hung et al. 2014; Jorfi and Foster 2015). Kondo et al. reported a process to align of BNC in molecular ordered scaffolds. This allowed 3D-bottom up fabrication by controlling bacterial movement (Kondo and Kasai 2014; Kondo et al. 2002, 2012). An aqueous counter collision (ACC) method was also proposed for providing a single nanofiber from BNC pellicle of *G. xylinus* (Kose et al. 2011; Kondo et al. 2014).

The ACC method uses two opposing high-speed water jets containing BNC pellicle. It can provide ACC-BNC of approximately 30–70 nm in width, with a nearly constant aspect ratio of 100 (Kose et al. 2011). During ACC treatment, energy generated in counter collision disrupts weak molecular interactions such as *van der Waals* forces. The pellicle becomes pulverized into separate nanofibers. When native cellulose fibers are subjected to ACC treatment, hydrophobic glucan sheets composed of hydrogen-bonded anhydroglucose units become exposed on the surface of ACC-nanocellulose. Therefore, ACC-BNC surface also exhibits hydrophobicity in addition to hydrophilicity from hydroxy groups, leading to amphiphilicity (Tsuboi et al. 2014). Kose and Kondo reported that ACC treatment could transform the meta-stable cellulose I_α phase into the stable I_β phase, without decreasing the overall crystallinity.

In the current study, the surface properties of ACC-BNC were investigated through interactions with poly(vinyl alcohol) (PVA) (Nishio et al. 1989; Kondo et al. 1994). The effects of these interactions with dependence on the crystalline phase of the nanocellulose surface were then elucidated. Varieties in theses interactions were assumed to correspond to differences in the crystallization of PVA. Therefore, the characteristics of PVA could be used as a probe, when PVA was mixed with ACC-BNC during ACC treatment (hereafter referred to as on-site ACC). This thermodynamic probe revealed the surface effects of ACC-BNC containing I_α and I_β crystalline phases that were altered during ACC-treatment. This study compares the different surface characteristics of ACC-nanocellulose and ACC-BNC, which depended on the I_β-rich or I_α-involved phases.

Experimental

Preparation of BNC aqueous suspension and PVA aqueous solution

Schenk and Hildebrandt (SH) medium was used to culture *G. xylinus* (NQ-5: ATCC 53582) to obtain the pellicle (Hestrin and Schramm 1954). The components of the SH medium were: D-glucose and critic acid of culture grade, purchased from Wako Pure Chemicals Co., Ltd., Tokyo, Japan; di-sodium hydrogen phosphate heptahydrate of culture grade purchased from Nacalai Tesque Inc., Osaka, Japan; yeast extract and peptone purchased from Becton, Dickinson and Co., NJ, USA. Ultra pure water (MilliQ water) used as the solvent.

Strains of *G. xylinus* were statically activated in SH medium at 30 °C for 3 days. They were subsequently cultured in fresh SH medium in sterilized polypropylene container at 30 °C for 2 weeks, to obtain gel-like film of the pellicle sheet, which had a thickness approximately 1 cm. The film was wrapped at the air–liquid interface of the culture medium. The pellicle was washed in ultra pure water for 5 days. To remove residue protein and bacterial cell, the sheet was then immersed in 0.1 wt% aqueous sodium hydroxide at 80 °C for 4 h. The pellicle was then washed in ultra pure water again for 3 days until a pH of approximately 7 was obtained.

The purified pellicle sheet was cut into cubes of no larger than approximately 1 cm^3, using clean scissors. One hydrogel cubes was transferred into a dry oven, for measuring the weight concentration (wt%) of cellulose. Other hydrogel cubes were dispersed in deionized water, and pulverized using a homogenizer, Physcotron NS-51 (Microtec Co., Ltd., Chiba, Japan) for less than 5 min at 20,000 rpm, to yield an 0.4 wt% BNC aqueous suspension.

PVA (M_w = 31,000–50,000, 98% saponified, Sigma-Aldrich Co., Ltd., Osaka, Japan) was further

saponified using 0.1 M sodium hydroxide aqueous solution, to achieve a PVA purification of 99.9%. Dried PVA powder was dissolved in ultra pure water at 90 °C at 1.2 wt%.

On-site ACC treatment: separation of a single nanofiber from pellicle and simultaneous mixing with PVA

It was difficult to mix the ACC-BNC aqueous suspension and PVA aqueous solution by simple stirring, because they gradually phase-separated over time. Therefore, the ACC process was used to mix BNC and PVA at the nanoscale, and is referred to as on-site ACC. Prior to on-site ACC treatment, the pre-treated BNC aqueous suspension and saponified PVA aqueous solution were mixed by stirring overnight. The cellulose weight fraction in the mixture was controlled in the range of 10–60%. The aqueous mixture was then loaded into the ACC system (CNNT Co. Ltd., Seoul, South Korea) at ejection pressures of 120, 160, and 200 MPa with 30 *Pass* (i.e. the number of repeated counter collisions in the cycling ACC operation).

Fractions of the resulting aqueous suspensions were cast to obtain nanocomposite films, by pouring into polyethylene cups, and subsequently degassing overnight using a water aspirator in a 50 °C water bath. The suspension was placed in a dry oven at 50 °C for casting.

Transmission electron microscopy observations of ACC-BNC

Immediately after ACC treatment, the composite aqueous suspensions were diluted with ultra pure water and sonicated for 10 s at 25 °C with minimum frequency under 400 W by using ultrasonic generator 400-28F (Kaijo Co. Ltd., Tokyo, Japan). The suspensions were then mixed with 0.2 wt% aqueous uranyl acetate for negative staining. This mixture was then diluted to 0.1% uranyl acetate, and droplets were deposited on copper grids covered with formvar. The samples were air-dried at room temperature before being observed with transmission electron microscopy (TEM), to evaluate the shape and width of the fibers. The average width was calculated from the TEM images of 50 cellulose fibers.

Density measurements of nanocomposite films

The specific densities (d) of cast films were measured by pycnometry, to determine the volume fractions of cellulose fibers in the composites. *p*-Xylene (0.86 g/cm^3, Wako Co., Ltd., Tokyo, Japan) and tetrachloromethane (1.59 g/cm^3, Wako Co., Ltd., Tokyo, Japan) were used for the density measurements at 25 °C.

Volume fractions of ACC-BNC in the nanocomposite

When considering the interaction between ACC-BNC and PVA, only the surface (skin) of the ACC-BNC fiber was assumed to interact with PVA. Thus, the surficial volume of the ACC-BNC nanofibers ($V_{NC\text{-}sur}$) was calculated by approximating the ribbon-like ACC-BNC as a four-sided prism:

$$V_{NC-sur} = (\text{Skin volume of single ACC-BNC}) \times (\text{ACC-BNC number}) \quad (1)$$

$$\therefore V_{NC-sur} = \left\{ w^2 \cdot l - (w - 2t)^2 \cdot l \right\} \times \frac{W_{com} \cdot f}{w^2 \cdot l \cdot d_{cell}} \quad (2)$$

where w is observed width of the ACC-BNC, l is the length of the nanocellulose, t is the effective skin thickness which was 0.66 nm, W_{com} is total weight of nanocomposite, f is weight fraction of ACC-BNC, and d_{cell} is the density of ACC-BNC. Based on the previous study (Kose et al. 2011), the d_{cell} value was estimated as mean value of the densities of the cellulose I_α phase and I_β phases, with a $d_{cell} = 1.62$ g/cm^3. The nanocellulose aspect ratio was considered to be 100 and was used to estimate the nanocellulose length from the width observed TEM images.

To investigate how the surface of ACC-BNC interacted with PVA, the calculated surface volume of the ACC-nanocellulose components ($V_{NC\text{-}sur}$) was used for comparing thermodynamic index. The surface volume fraction was estimated by:

$$V_{NC-sur}/V_{com} = \left[\left\{ w^2 \cdot l - (w - 2t)^2 \cdot l \right\} \times \frac{W_{com} \cdot f}{w^2 \cdot l \cdot d_{cell}} \right] \Big/ \times \left(\frac{W_{com}}{d} \right) \quad (3)$$

Thus, the following Eq. (4) is obtained

$$V_{NC-sur}/V_{com} = \frac{w^2 \cdot l - (w - 2t)^2 \cdot l}{w^2 \cdot l} \frac{d \cdot f}{d_{cell}} \quad (4)$$

where V_{com} is total volume of the nanocomposite.

Differential scanning calorimetory measurements

To investigate the interfacial interaction of ACC-BNC and PVA, differential scanning calorimetry (DSC) measurements were performed on approximately 5 mg of the PVA component in the composite, under a nitrogen atmosphere using a Perkin-Elmer DSC-7 instrument (PerkinElmer, Inc., Waltham, MA, USA). The instrument was calibrated with an indium standard. The equilibrium melting point (T_m^{eq}) of PVA mixed with ACC-nanocellulose was determined from DSC measurements as follows. Film samples containing approximately 5 mg of PVA were placed in aluminum sample pans, which were then heated to 235 °C and maintained at this temperature for 5 min, to eliminate any PVA crystalline residues, because the T_m^{eq} of the purified PVA was 239.20 °C. The samples were then quenched to the selected isothermal crystallization temperature, and held at this temperature for 7 h to allow complete crystallization. The samples were then cooled to 20 °C. After each sample was isothermally crystallized, the melting point was then measured using a heating rate of 10 °C/min. Hoffman–Weeks plots of the melting points were then obtained (Hoffman and Weeks 1962), from which the equilibrium melting point was determined for each film.

Results and discussion

ACC-BNC obtained from on-site ACC treatment

BNC dispersed in PVA aqueous solution was used in the on-site ACC treatment, which pulverized the BNC and mixed it with PVA at the nanoscale. The resulting homogeneous milky aqueous mixture exhibited no phase separation. The crystalline phase ratio (i.e. I_α/I_β ratio) of the ACC-BNC was considered to depend on the ACC ejection pressure. Sample preparation pressures and results of TEM observations and film density measurements are listed in Table 1.

The TEM images in Fig. 1 show that single nanocellulose fibers of different widths could be prepared by varying the ACC ejection pressure. Average nanocellulose fiber widths and standard deviations are listed in Table 1.

ACC-BNC obtained from on-site ACC treatment existed as ribbon-like single nanofibers. However, the thicker ACC-nanocellulose fibrils were often entangled (Fig. 1c, inset). This variation in morphology affected the measured average width, as shown by the associated standard deviations in Table 1. Thinner single ACC-BNC fibers exhibited a smaller standard deviation in their measured average width.

BNC pulverized by conventional ACC treatment without PVA reportedly yielded ACC-nanocellulose with widths of 18 ± 9 and 35 ± 19 nm, at ejection pressures of 200 and 100 MPa, respectively (Kose and Kondo 2013). The width of the current ACC-BNC was 5–50 nm, which was comparable with, or slightly thinner than, the ACC-BNC prepared without PVA.

ACC-BNC surface characteristics determined from PVA crystallization behavior

ACC treatment can change the crystalline phase ratio of BNC, without decreasing the overall crystallinity. I_α is the major crystalline structure of BNC, and reportedly changed to I_β upon ACC treatment (Kose et al. 2011). The current on-site ACC treatment was also expected to change the initial cellulose I_α phase of BNC to I_β. The surface characteristics of ACC-BNC were investigated by monitoring the PVA crystallization behavior in the nanocomposite films. The T_m^{eq} of crystalline polymer components generally decreases when forming attractive interactions with other substances. Interactions between ACC-BNC and PVA were therefore expected to decrease the T_m^{eq} of the crystalline PVA component.

Melting point of crystalline polymer is usually dependent on the crystallization temperature. Therefore, PVA crystallization was compared by equilibrium melting point, which was obtained from Hoffman–Weeks plots of isothermally crystallized PVA (Hoffman and Weeks 1962). The T_m^{eq} values differed to that of neat PVA, 239.2 °C. The T_m^{eq} is plotted against the cellulose volume fraction of the nanocomposites in Fig. 2.

Table 1 Film densities of ACC-BNC/PVA nanocomposites

ACC-BNC (with ACC ejection pressure)	Width (nm)	S.D. (nm)	Weight fraction of ACC-BNC (%)	Composite density (g/cm^3)
ACCBC-120 MPa	52.42	17.90	20	1.375
	35.07	23.19	10	1.314
	17.39	2.88	50	1.427
	17.34	8.80	30	1.379
	17.13	6.08	40	1.384
ACCBC-160 MPa	41.23	11.57	20	1.368
	20.19	15.83	10	1.310
	15.49	2.98	40	1.382
	9.23	3.65	50	1.419
	5.51	1.47	30	1.367
ACCBC-200 MPa	40.18	6.58	20	1.356
	17.10	5.28	10	1.299
	12.76	1.44	40	1.363
	4.17	0.79	60	1.413

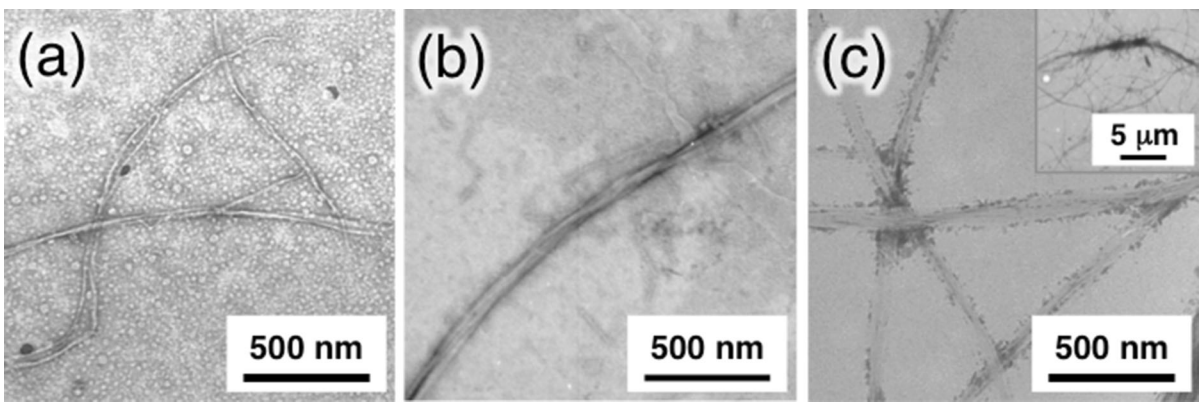

Fig. 1 TEM images of negatively stained ACC-nanocelluloses fibers with width of **a** 4.17 nm, **b** 17.10 nm, and **c** 35.07 nm. The inset image in **c** shows a lower magnification of a single ACC-nanocellulose fibril. The PVA component was also negatively stained

In Fig. 2, the T_m^{eq} of ACC-BNC is categorized according to the ACC ejection pressure used during on-site ACC. A change in the I_α/I_β ratio in the ACC-nanocellulose was initially assumed to correlate with the magnitude of the ACC ejection pressure. The trends in the three T_m^{eq} plots were generally comparable. However, the ACCB-200MPa sample contained many thinner ACC-BNC fibers, and showed slightly different behavior. The ACC-BNC categorization in Fig. 2 was therefore revised based on the ACC-BNC width.

The ACC-BNC groups were re-categorized by their width. Specifically, the ACCB-S and ACCB-L groups contained fibers of < 15 and 15–50 nm in width, respectively. These new plots are shown in Fig. 3. The T_m^{eq} of the crystalline PVA component increased with increasing amount of ACCB-L. This tendency seems to be a typical behavior for compositions of a crystalline polymer and nucleating agent. In contrast, the T_m^{eq} of PVA slightly decreased with increasing amount of ACCB-S, which is characteristic of ACCB-S acting as a diluent for PVA (Nishio et al. 1989; Kondo et al. 1994; Sawatari and Kondo 1999.). The opposite two phenomena are estimated to occur with dependence on fraction occupied by interface ACC-

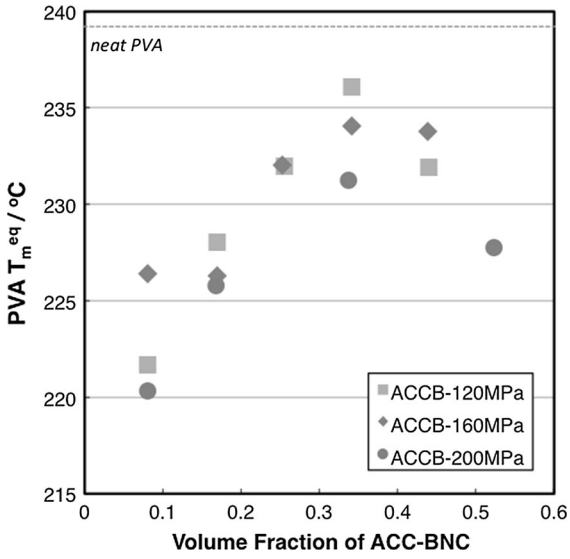

Fig. 2 Equilibrium melting point (T_m^{eq}) of the PVA components as a function of cellulose volume fraction, for ACC-BNC categorized by ACC ejecting pressure. The dashed line indicates T_m^{eq} of neat PVA, 239.2 °C

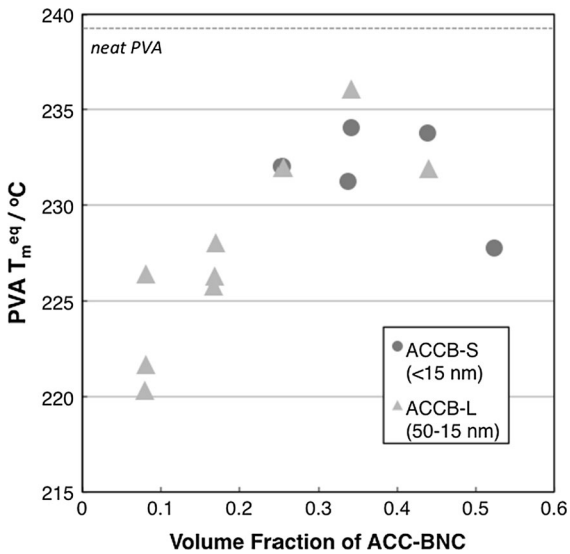

Fig. 3 Equilibrium melting point (T_m^{eq}) of the PVA component as a function of cellulose volume fraction, for ACC-BNC categorized by its nanofiber width. The dashed line indicates T_m^{eq} of neat PVA, 239.2 °C

BNC in PVA. Thus, the volume fraction of ACC-BNC was required to be calculated without the contribution of the inner nanocellulose domain, as described in the "Experimental" section Eq. (4).

Figure 4 shows how the behavior of the PVA T_m^{eq} depended on the ACC-BNC width. The T_m^{eq} of the PVA

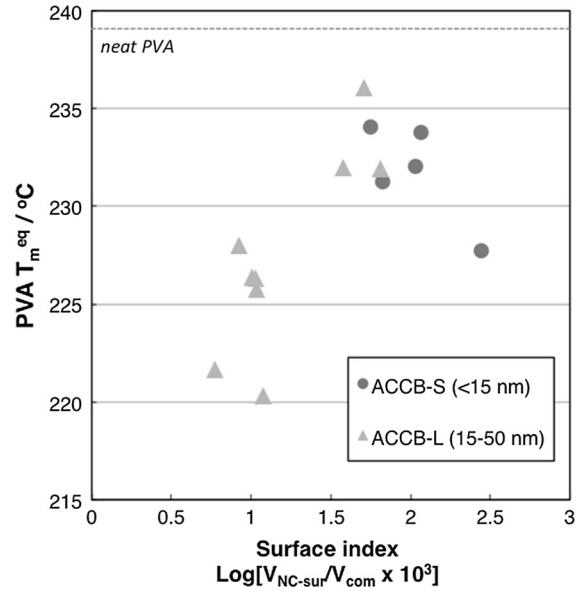

Fig. 4 T_m^{eq} of PVA components against index representing surface volume fractions of three ACC-BNC with different widths

component mixed with ACCB-L significantly increased with increasing nanocellulose surface volume fraction (surface index). In contrast, the T_m^{eq} decreased proportionally with increasing total surface amount of ACCB-S in the PVA matrix.

The changes in T_m^{eq} with fiber width can be explained as follows. The changes in the melting points for isothermally crystallized PVA samples indicated interfacial interactions between the components in the nanocomposites. For thicker samples such as ACCB-L, the T_m^{eq} increased with increasing surface volume fraction of ACC-nanocellulose (Fig. 4). This behavior was considered to result from a nucleating effect. The surfaces of ACCB-L were likely to provide scaffolds for the epitaxial growth of PVA. In contrast, increasing the surface volume fraction of the thinner ACCB-S enhanced the interactions between the ACC-nanocellulose and PVA, which decreased the T_m^{eq}. The effect of the ACCB-S surface was similar to that of a diluent.

The ACC-BNC exhibited nanoscale effects. Nanoscale effects depending on the width of ACC-BNC have been reported for ACC-BNC/poly(lactic acid) (PLA) nanocomposites (Kose and Kondo 2013). The amphiphilic ACC-BNCs with width of appropriately 60 nm enhanced the crystallization rate of PLA. Kose and Kondo suggested that "the smaller, the better"

rule did not always apply in this case. In the current study, the width of ACC-BNC acting as a nucleating agent for PVA was 15–50 nm (ACCBC-L in Fig. 4). PVA or PLA epitaxial nucleation on the ACC-BNC surface scaffold may have been optimized at a fiber width of approximately 50–60 nm.

Dependence of crystalline phases on thermodynamic Interactions

Thicker ACCB-L had a nucleating effect on PVA, while thinner ACCB-S acted as a diluent for PVA. To better understand the interaction between ACC-BNC and PVA, the interaction parameter (χ_{12}) was used, in an extension of the Flory–Huggins approximation (Flory 1953). Scott proposed an equation for the thermodynamic decrease of the melting point caused by a diluent (Scott 1949):

$$1/T_m - 1/T_m^0 = -R\frac{V_{2u}}{\Delta H_{2u}}\left\{\frac{\ln v_2}{V_2} + \left(\frac{1}{V_2} - \frac{1}{V_1}\right)v_1 + \frac{Bv_1^2}{RT_m}\right\} \quad (2-1)$$

where T_m^0 is the melting point of neat PVA (= 512.36 K, 239.20 °C), T_m is the observed T_m^{eq} for PVA mixed with a diluent, R is the gas constant [1.987 cal/(mol K)], subscripts *1* and *2* indicated the non-crystallizable and crystalline components, respectively, v_1 and v_2 are the volume fractions; V_1 and V_2 are the molar volumes; V_{2u} is the molar volume of a repeating unit of 2; and ΔH_{2u} is the enthalpy of fusion per mole of repeating unit of 2.

ACC-BNC and PVA were assumed to be the non-crystallizable and crystalline components, respectively. When V_1 and V_2 are 1×10^4–1×10^6, the entropy term in Eq. (2-1) can be entirely neglected (Imken et al. 1976). The degree of polymerization of cellulose molecules in ACC-nanocellulose was estimated to be 200–250 because covalent bonds in the starting material (BNC) cannot be cleaved by the provided ACC energy. V_1 was estimated to be approximately 3×10^5. The M_w of PVA was 31,000–50,000, and V_2 was approximately 3×10^6. Equation (2-1) can therefore be rearranged to Eq. (2-2), from which the enthalpic contribution to the melting point depression can be evaluated:

$$\Delta T_m^{eq} = -T_m^0 \frac{V_{2u}}{\Delta H_{2u}} Bv_1^2 \quad (2-2)$$

$\Delta H_{2u}/V_{2u}$ for the PVA component was calculated to be 45.4 cal/cm^3 (Nishio et al. 1989). Equation (2-2) is related to the parameter B, which indicates the interaction energy density characteristics of the two components. The interaction parameter, (χ_{12}) is described as

$$\chi_{12} = \frac{BV_{1u}}{RT} \quad (2-3)$$

The molar volume of cellulose per repeating unit, V_{1u}, is 107 cm^3/mol, therefore χ_{12} at 512.36 K can be calculated:

$$\chi_{12} = \frac{B \times 107}{1.987 \times 512.36} \quad (2-3')$$

For the ACCB-S/PVA nanocomposite, the volume fraction of the nanocellulose component (v_1) is considered to be the ratio of the cellulose volume to the entire composite volume. The nanocellulose volume fraction was then used to calculate the values of B and χ_{12}, which are listed in Table 2.

Negative values of B and χ_{12} indicate attractive interactions between the two components. The data in Table 2 indicated that the ACCB-S surface interacted well with PVA. Two sets of data were selected as references. One was ACC-nanocellulose derived from wood cellulose having stable cellulose I_β surface (unpublished data). The other was values for cellulose/PVA molecular blends.

Compared with the wood ACC-nanocellulose/PVA nanocomposite, ACC-BNC had a weaker interaction with PVA. The ACC-BNC surface differed from the surface state of ACC-nanocellulose since it contained exposed cellulose I_β phases. Kose et al. reported that crystalline structure of ACC-BNC appeared to be a composition of cellulose I_α and I_β. Therefore, the surface of ACC-BNC was not completely covered with cellulose I_β phase. ACC-BNC may have also cellulose I_α on its surface, although this was difficult to quantify.

ACC-nanocellulose had two driving forces for its surficial properties in the presence of PVA: surface free energy and hydrogen bonding. The calculated B and χ_{12} were associated with hydrogen bonding. Hydrogen bonding is considered to contribute to form an interaction of PVA with cellulose, which finally

Table 2 Interaction energy density and interaction parameter for ACC-nanocellulose with PVA

	Interaction energy density, B (cal/cm^3)	Interaction parameter, χ_{12}
ACCB-S (BNC)/PVA (at 512 K)	− 1.63	− 0.171
ACC-nanocellulose (wood)/PVA (at 512 K) (unpublished data)	− 12.15	− 1.27
Cellulose/PVA molecular blend (at 513 K) (Nishio et al. 1989)	− 9.38	− 0.985

Table 3 Efficiency of ACC-nanocellulose as nucleating agent for PVA

Derivation of ACC-nanocelluose	Crystalline phase	Volume fraction	T_m^{eq} of PVA (°C)	Change rate (ΔT_m/V.F.)
Microcrystalline cellulose (wood)	I_β rich	0.026–0.126: Δ 0.1	234.1–236.22: Δ 2.12	2.1 °C/0.1%
BNC	$I_\alpha + I_\beta$	0.081–0.341: Δ 0.26	221.68–236.08: Δ 14.4	5.5 °C/0.1%

assists to allow cellulose as a diluent for PVA. When an effect of hydrogen bonding of ACC-nanocellulose was weaker than surface free energy, the nanocellulose surface may have been a better scaffold for epitaxial crystalline growth. The cellulose I_α plane had better potential to act as a nucleating agent than the cellulose I_β surface, because the crystal lattice of I_α was well matched with the lattice parameter of PVA (Urushihara et al. 2009). Hence, ACC-BNC was a better nucleating agent than ACC-nanocellulose derived from I_β-dominant wood cellulose. ACC-nanocellulose of wood cellulose was a poorer nucleating agent for PVA than ACC-BNC (Table 3). In summary, the dependence of crystalline phases upon thermodynamic interactions was apparent at the interface between ACC-nanocellulose and PVA.

Conclusion

Bacterial nanocellulose pellicle was separated into single nanocellulose fibers (ACC-BNC), by on-site ACC treatment and simultaneous mixing with aqueous PVA. ACC treatment could transform the major crystalline structure I_α of BNC to I_β. The equilibrium melting point of PVA in the nanocomposite was used as a probe to investigate the dependence of surface crystalline phases on thermodynamic interactions. Changes in the equilibrium melting point of PVA were observed, indicating interactions between ACC-BNC and PVA. These changes depended on the width of the ACC-BNC fibers. ACC-BNC fibers of approximately 17–50 nm in width acted as a nucleating agent for PVA. ACC-BNC fibers thinner than 15 nm acted as a diluent of PVA. This trend was opposite to the case for I_β-dominant ACC-wood nanocellulose. A detailed comparison of the thermodynamic interactions between ACC-BNC and ACC-wood nanocellulose was therefore required. The interaction parameter indicated that the ACC-BNC and PVA interface was likely to be less thermodynamically stable than the ACC-wood nanocellulose and PVA interface. This was because the ACC-BNC surface contained both I_β and I_α phases, even after ACC-treatment. The decrease in equilibrium melting point of PVA was larger for ACC-BNC than for ACC-wood nanocellulose. This indicated that ACC-BNC was a better nucleating agent. I_α crystalline phases may have more potential than I_β phases as scaffolds for the epitaxial growth of PVA. The ACC method was therefore capable of tailoring the nanofiber surface.

References

Atalla RH, Vanderhart DL (1984) Native cellulose: a composite of two distinct crystalline forms. Science 223(4633): 283–285

Flory PJ (1953) Principles of polymer chemistry. Cornell University Press, Ithaca, pp 568–571

Helenius G, Backdahl H, Bodin A, Nannmark U, Gatenholm P, Risberg B (2006) In vivo biocompatibility of bacterial cellulose. J Biomed Mat Res Part A 76A(2):431–438

Hestrin S, Schramm M (1954) Synthesis of cellulose by *Acetobacter xylinum.2*. Preparation of freeze-dried cells

capable of polymerizing glucose to cellulose. Biochem J 58(2):345–352
Hoffman JD, Weeks JJ (1962) Melting process and equilibrium melting temperature of polychlorotrifuluoroethylene. J Res Natl Bur Stand Sect A Phys Chem 66(JAN-F):13–28
Huang Y, Zhu C, Yang J, Nie Y, Chen C, Sun D (2014) Recent advances in bacterial cellulose. Cellulose 21(1):1–30
Ifuku S, Nogi M, Abe K, Handa K, Nakatsubo F, Yano H (2007) Surface modification of bacterial cellulose nanofibers for property enhancement of optically transparent composites: dependence on acetyl-group DS. Biomacromol 8(6):1973–1978
Imken RL, Paul DR, Barlow JW (1976) Transition behavior of poly(vinylidene fluoride)/poly(ethyl methacrylate) blends. Polym Eng Sci 16(9):593–601
Jorfi M, Foster EJ (2015) Recent advances in nanocellulose for biomedical applications. J Appl Polym Sci 132(14):41719
Klemm D, Kramer F, Moritz S, Lindstrom T, Ankerfors M, Gray D, Dorris A (2011) Nanocelluloses: a new family of nature-based materials. Angew Chemi Int Ed 50(24):5438–5466
Kondo T, Kasai W (2014) Autonomous bottom-up fabrication of three-dimensional nano/microcellulose honeycomb structures, directed by bacterial nanobuilder. J Biosci Bioeng 118(4):482–487
Kondo T, Sawatari C, Manley RS, Gray DG (1994) Characterization of hydrogen bonding in cellulose-synthetic polymer blend systems with regioselectively substituted methylcellulose. Macromolecules 27(1):210–215
Kondo T, Nojiri M, Hishikawa Y, Togawa E, Romanovicz D, Brown RM (2002) Biodirected epitaxial nanodeposition of polymers on oriented macromolecular templates. PANS 99(22):14008–14013
Kondo T, Kasai W, Nojiri M, Hishikawa Y, Togawa E, Romanovicz D, Brown RM (2012) Regulated patterns of bacterial movements based on their secreted cellulose nanofibers interacting interfacially with ordered chitin templates. J Biosci Bioeng 114(1):113–120
Kondo T, Kose R, Naito H, Kasai W (2014) Aqueous counter collision using paired water jets as a novel means of preparing bio-nanofibers. Carbohydr Polym 112:284–290
Kose R, Kondo T (2013) Size effects of cellulose nanofibers for enhancing the crystallization of poly(lactic acid). J Appl Polym Sci 128(2):1200–1205
Kose R, Mitani I, Kasai W, Kondo T (2011) "Nanocellulose" as a single nanofiber prepared from pellicle secreted by gluconacetobacter xylinus using aqueous counter collision. Biomacromol 12(3):716–720
Moon RJ, Martini A, Nairn J, Simonsen J, Youngblood J (2011) Cellulose nanomaterials review: structure, properties and nanocomposites. Chem Soc Rev 40(7):3941–3994
Nishio Y, Haratani T, Takahashi T (1989) Cellulose/poly(vinyl alcohol) blends: an estimation of thermodynamic polymer-polymer interaction by melting point depression analysis. Macromolecules 22(5):2547–2549
Sawatari C, Kondo T (1999) Interchain hydrogen bonds in blend films of poly(vinyl alcohol) and its derivatives with poly(ethylene oxide). Macromolecules 32(6):1949–1955
Scott RL (1949) The thermodynamics of high polymer solutions. V. Phase equilibria in the ternary system: polymer 1—polymer 2—solvent. J Chem Phys 17(3):279–284
Shah N, Ul-Islam M, Khattak WA, Park JK (2013) Overview of bacterial cellulose composites: a multipurpose advanced material. Carbohydr Polym 98(2):1585–1598
Tsuboi K, Yokota S, Kondo T (2014) Difference between bamboo- and wood-derived cellulose nanofibers prepared by the aqueous counter collision method. Nord Pulp Res J 29(1):69–76
Urushihara T, Okada K, Watanabe K, Toda A, Kawamoto N, Hikosaka M (2009) Acceleration mechanism in critical nucleation of polymers by epitaxy of nucleating agent. Polym J 41(3):228–236
Vitta S, Thiruvengadam V (2012) Multifunctional bacterial cellulose and nanoparticle-embedded composites. Cur Sci 102(10):1398–1405
Wada M, Okano T, Sugiyama J (1997) Synchrotron-radiated X-ray and neutron diffraction study of native cellulose. Cellulose 4(3):221–232
Yamamoto H, Horii F, Hirai A (1996) In situ crystallization of bacterial cellulose. 2. Influences of different polymeric additives on the formation of celluloses I-alpha and I-beta at the early stage of incubation. Cellulose 3(4):229–242
Yamanaka S, Watanabe K, Kitamura N, Iguchi M, Mitsuhashi S, Nishi Y, Uryu M (1989) The structure and mechanical properties of sheets prepared from bacterial cellulose. J Mat Sci 24(9):3141–3145
Yano H, Sugiyama J, Nakagaito AN, Nogi M, Matsuura T, Hikita M, Handa K (2005) Optically transparent composites reinforced with networks of bacterial nanofibers. Adv Mater 17(2):153–155